Tracer redistribution by clouds in West Africa: Numerical modeling for dry and wet seasons

M. Renard, N. Chaumerliac, S. Cautenet, E. Nickerson

JOURNAL OF GEOPHYSICAL RESEARCH, VOL. 99, NO. D6, PAGES 12,873–12,883, JUNE 20, 1994

Tracer redistribution by clouds in West Africa: Numerical modeling for dry and wet seasons

M. Renard, N. Chaumerliac, and S. Cautenet
LAMP/OPGC, Université Blaise Pascal, Aubiere, France

E. C. Nickerson
National Oceanic and Atmospheric Administration/FSL, Boulder, Colorado

Abstract. The vertical transport by clouds of an inert tracer and its redistribution by complex West African circulations are examined using a two-dimensional mesoscale meteorological model with explicit microphysics. The model reproduces the tropical distribution of clouds and precipitation along a meridional cross section over West Africa, corresponding to the position of the Intertropical Convergence Zone (ITCZ) during the dry and rainy seasons. The resulting redistribution of the inert tracer is therefore closely related to the northward migration of the ITCZ between January and July. The occurrence of biomass burning during the dry season is shown to be an important source of tracer enrichment at upper levels in the atmosphere.

1. Introduction

Emissions from biomass burning in intertropical regions have been shown to contribute to the global redistribution of atmospheric trace gases and hence may be expected to play an important role in global climate change [*Delmas*, 1982; *Crutzen et al.*, 1985; *Harris et al.*, 1988]. Tropical atmospheric chemistry has been studied extensively during the Amazon Boundary Layer Experiment (ABLE 2A) (described by *Garstang et al.*, 1988], over West Africa during the TROPOZ I experiment (Tropospheric Ozone Experiment) (*Marenco et al.*, 1990] and also during DECAFE (Dynamique et Chimie de l'Atmosphère en Forêt Équatoriale) (reported in a special issue of the *Journal of Geophysical Research*, *97*(D6), 1992). These experiments, especially DECAFE, have highlighted the difficulty of separating the interactive roles of fluxes, transport, and chemical reactions in the redistribution of chemical species in the troposphere.

Intertropical areas are of interest for three reasons:

1. Biogenic emissions from the equatorial forest and the occurrence of biomass burning during the dry season are sources of chemical compounds that are important in the global tropospheric chemistry budget.
2. The synoptic meteorology of West Africa is greatly influenced by the seasonal migration of the Intertropical Convergence Zone (ITCZ) and the associated African easterly jet (AEJ) located at an altitude of approximately 3.5 km. The dry and wet seasons are also marked by the presence of the south tropical jet (STJ), and the tropical easterly jet (TEJ) in January and July, respectively, at an altitude of 15 km.
3. These regions are subject to extensive convective activity associated with the shift of the ITCZ.

Both observations and theory emphasize the important role of convective clouds in redistributing trace gases in the atmosphere [*Chatfield and Crutzen*, 1984; *Chatfield and Delany*, 1990]. The chemistry of West African tropics is therefore very dependent on the extensive convective activity normally associated with the ITCZ and also on the intense and persistent airflow regimes that occur over West Africa.

The aim of this paper is to examine the interactions between chemistry and meteorology over West Africa by restricting the scope of the problem to the transport of an inert tracer. The resulting trace gas concentrations and their vertical profiles are therefore due solely to dynamical processes, thereby setting aside, for the moment, processes such as wet removal, deposition, and photochemistry.

The meteorological fields were obtained from a two-dimensional primitive equation model described in section 2. Our aim here is not to study the dynamics of meteorological circulations over West Africa but rather to reproduce the primary features of the observed wind fields that are responsible for species transport. The meteorological fields were initialized with an analytical procedure (section 3) to obtain a coherent representation of the field gradients instead of from the sparse and irregular data available over West Africa. Section 4 then examines the evolution of an inert tracer distribution over West Africa for both dry and wet seasons.

2. Model Description

To model West African circulations, we have adapted a two-dimensional version of the three-dimensional model of *Nickerson et al.* [1986]. The two-dimensional model domain extends from the 10°S to the 35°N in latitude and is a cross section around 0° longitude. The positive x and y axis are, respectively, toward the East and the North.

2.1. Model Equations

The model is a hydrostatic primitive equation model in which the grid system is staggered both horizontally and vertically. The vertical coordinate, ν, is defined by

$$\sigma = \frac{(p - p_t)}{\pi} = \frac{(4\nu - \nu^4)}{3} \quad (1)$$

Paper number 94JD00408.
0148-0227/94/94JD-00408$05.00

where

$$\pi = p_s - p_t \tag{2}$$

and p_s and p_t are the pressures at the surface and at the top of the model, respectively. The vertical resolution is constant in the ν coordinate, thus it varies from a few meters near the surface up to a kilometer or more in the highest vertical levels of the model [*Nickerson et al.*, 1986]. With respect to the horizontal resolution it is taken constant, equal to 40 km.

For the south-north component, v, and the west-east component, u, of the wind velocity, we define the variables $U = \pi u$ and $V = \pi v$. We split them into a forcing term and a perturbed term:

$$V = V_{\text{def}}(x, y, \nu) + V_{\text{div}}(y, \nu) + V'(y, \nu, t) \tag{3}$$

$$U = U_{\text{def}}(x, y, \nu) + U'(y, \nu, t) \tag{4}$$

where U', V' correspond to the perturbed fields and V_{div} is a stationary divergent field. U_{def}, V_{def} represent a stationary nondivergent field of the deformation satisfying the relationship

$$\left(\frac{\partial U_{\text{def}}}{\partial x}\right)_\nu + \left(\frac{\partial V_{\text{def}}}{\partial y}\right)_\nu = 0. \tag{5}$$

In the two-dimensional cross section, $x = 0$, U_{def} is assumed to vanish (see the appendix for a mathematical description of the U_{def}, V_{def}, and V_{div}).

The four prognostic equations for U', V', H, and π and the five diagnostic equations used in the model or for analysis purposes are

$$\frac{\partial U'}{\partial t} = -\frac{\partial V_u}{\partial y} + 2u\frac{\partial V_{\text{def}}}{\partial y} - \frac{1}{\sigma'}\frac{\partial (U\sigma'\dot{\nu})}{\partial \nu} + f_y(V_{\text{div}} + V') + \pi F_{H,U} + \pi F_{V,U} \tag{6}$$

$$\frac{\partial V'}{\partial t} = -\frac{\partial Vv}{\partial y} + v\left(\frac{\partial V_{\text{def}}}{\partial y}\right) - \frac{1}{\sigma'}\frac{\partial (V\sigma'\dot{\nu})}{\partial \nu} - f_y U' - RT_v\frac{\sigma\pi}{p}\frac{\partial \pi}{\partial y} - \pi\frac{\partial \Phi}{\partial y} + \pi F_{H,V} + \pi F_{V,V} + \pi F_f \tag{7}$$

$$\frac{\partial \pi H}{\partial t} = -\frac{\partial VH}{\partial y} + H\left(\frac{\partial V_{\text{def}}}{\partial y}\right) - U'\frac{\partial H}{\partial x} - \frac{1}{\sigma'}\frac{\partial (\pi H\sigma'\dot{\nu})}{\partial \nu} + \pi F_{H,H} + \pi F_{V,H} \tag{8}$$

$$\frac{\partial \pi}{\partial t} = -\int_0^1 \left(\frac{\partial V_{\text{div}}}{\partial y} + \frac{\partial V'}{\partial y}\right)\sigma'\, d\nu \tag{9}$$

$$\dot{\nu} = -\frac{1}{\pi\sigma'}\int_0^\nu \sigma'\left(\frac{\partial \pi}{\partial t} + \frac{\partial V_{\text{div}}}{\partial y} + \frac{\partial V'}{\partial y}\right) d\nu \tag{10}$$

$$\frac{\partial \Phi}{\partial \ln p} = -RT_v\left(1 + \frac{q_l + q_r}{1 + q_v}\right)^{-1} \tag{11}$$

$$w = \frac{1}{g}\left(\frac{\partial \Phi}{\partial t} + v\frac{\partial \Phi}{\partial y} + f_y\frac{uV_{\text{def}}}{\pi} + \dot{\nu}\frac{\partial \Phi}{\partial \nu}\right) \tag{12}$$

$$p = \rho RT_v \tag{13}$$

$$\frac{\partial H}{\partial x} = -\left(\frac{1}{T} + \frac{q_v}{C_pT}\left(\frac{dL_v}{dT} - \frac{L_v}{T}\right)\right) \cdot \frac{f_y p}{R(1 + 0.61q_v)\pi^2}\frac{1}{\sigma'}\frac{\partial V_{\text{def}}}{\partial \nu} \tag{14}$$

where $\dot{\nu} = (d\nu/dt)$ is the vertical velocity in the transformed coordinate system, and definitions of the other symbols are given in Table 1.

The forcing deformation field, U_{def}, V_{def}, is associated with a constant perturbation of the geopotential through geostrophic balance. Thus the vertical shear of V_{def} induces a zonal gradient of the temperature ($\partial T/\partial x$) (thermal wind relationship) and hence of the entropy ($\partial H/\partial x'$) as described in (14).

The water loading has been included in the hydrostatic equation (11) as a function of cloud water mixing ratio q_l and rainwater mixing ratio q_r [*Hsie et al.*, 1984].

The F_H horizontal diffusion terms are written as a fourth-order operator. The F_V terms represent the vertical turbulent mixing effects computed with the prediction model of

Table 1. Model Variables and Constants

Symbol	Definition
H	entropy
θ	potential temperature
q_v	vapor mixing ratio
q_l	cloud water mixing ratio
q_r	rainwater mixing ratio
T_v	virtual temperature $(1 + 0.61q_v)T$
T'_v	perturbation of virtual temperature
R	gas constant for dry air
p	pressure
p_t	pressure at the top of the model 10 hPa
p_s	pressure at the surface
π	p_s-p_t
ρ	air density
Φ	geopotential
Φ'	geopotential perturbation
f_y	Coriolis parameter: β(y-yequa)
β	2×10^{-11} m^{-1} s^{-1}
yequa	equator position on the y axis
C_p	specific heat at constant pressure for dry air
L_v	latent heat of evaporation for water
u	West-East wind component
v	South-north wind component
u', v'	u,v perturbations
U	πu
V	πv
U_{def}	deformation field for u
V_{def}	deformation field for v
V_{div}	divergent field for v
U'	U perturbation
V'	V perturbation
w	vertical velocity (cm s^{-1})
F_H	horizontal diffusion term
F_v	vertical turbulent mixing term
F_f	forcing term
K	turbulent vertical mixing coefficient
γ_{cg}	countergradient of temperature
ν	vertical coordinate of the model
σ	p_s-p_t/π
σ'	$d\sigma/d\nu$
$\dot{\nu}$	$d\nu/dt$
$C(z)$	tracer concentration at altitude z

the turbulent kinetic energy in the planetary boundary layer (PBL) described by *Mahfouf et al.* [1987]. These terms for any variable X are written as

$$\pi F_{V,X} = B \frac{\partial}{\partial \nu}\left(BK \frac{\partial \pi X}{\partial \nu}\right) \text{ with } B = -\frac{gp}{RT_v \pi \sigma'}.$$

The coefficients K are proportional to the square root of the turbulent kinetic energy and to the mixing length. This mixing length and the evolution of the turbulent kinetic energy are computed, using the results of *Therry and Lacarrère* [1983], everywhere in the troposphere. In fact, noticeable values of K are only found in the PBL.

To ensure a positive heat flux in regions of neutral stratification or slightly stable conditions, a countergradient of temperature is added to the $-K(\partial H/\partial z)$ term. Hence the $F_{V,H}$ term is written as

$$\pi F_{V,H} = B \frac{\partial}{\partial \nu}\left(BK\left(\frac{\partial \pi H}{\partial \nu} - \pi \gamma_{cg}\right)\right),$$

where γ_{cg} is proportional to the virtual sensible heat flux at the surface [*Therry and Lacarrère*, 1983]. This parameterization of the turbulent mixing effects enables convection to develop in synergy with the microphysics effects, although no parameterization of the convection is included in the model. The relative effects of the turbulence scheme versus the microphysical scheme have previously been discussed by *Chaumerliac et al.* [1992] for the case of frontal rain.

For the lateral boundaries, we have applied the method of *Davies* [1983], using the initial boundary values of the fields as constant forcing boundary conditions.

In (7) the F_f term is an additional forcing term proportional to the unperturbed meridional wind, $V_{\text{def}} + V_{\text{div}}$. This term has been added to force the convergence of the numerical evolution toward the observed meridional wind field. In fact, a three-dimensional model is required to properly represent the evolution of these regions. Our aim here is to reproduce the principal features of the meteorological fields over West Africa that are responsible for the transport of an inert tracer and not to study the dynamics of West African circulations.

To complete this basic version of the model, we have used the parameterization of the microphysics based upon the work of *Kessler* [1969] and described by *Richard and Chaumerliac* [1989]. This parameterization can be classified as explicit microphysics according to the definition given by *Hsie et al.* [1984].

2.2. Initialization Procedure

We assume that the meridional wind perturbation, v', vanishes at the beginning of the simulation. Hence the meridional wind reduces to the deformation and divergent winds, v_{def}, v_{div}.

The initial vapor mixing ratio distribution is prescribed as a function of the strong gradient of moisture of the intertropical front (section 3.1).

The initial perturbations of the virtual temperature, T'_v, and of the zonal component, u', of the wind are assumed to be balanced:

$$f_y u' = -\left(\frac{\partial \Phi'}{\partial y}\right)_p \tag{15}$$

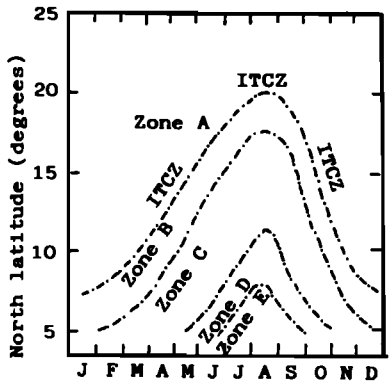

Figure 1. Intertropical convergence zone displacements in Walker's diagram: zone A, Saharan cloudless air; zone B, W-SW winds, shallow maritime air, thunderstorms; zone C, intense rainfalls associated with SW monsoon flow; zone D, stable, cold, and very cloudy atmosphere with continuous weak rainfalls; zone E, above the coastal lands only for a short period (July to September) accompanied by low temperatures and only few rains (reproduced from *Cautenet and Rosset* [1989]).

$$RT'_v = -\frac{\partial \Phi'}{\partial \ln p} \tag{16}$$

where Φ' is the initial perturbation of the geopotential.

Starting with an analytical function for $u'(y, p)$, we deduce from (15) and (16) the analytical expressions of Φ' and T'_v in pressure coordinate. Hence we obtain T'_v in the vertical coordinate system ν. Integrating (16) with the numerical scheme of the model, we deduce the numerical values of Φ. Finally, the numerically balanced values of u' are computed with the horizontal discretization scheme of the model for (15). In the following section, these initial fields are presented in more detail.

3. Meteorological Fields

Since meteorological processes such as the vertical transport within clouds may have a profound effect on atmospheric chemistry, it is necessary to depict the primary circulation features over West Africa as accurately as possible.

Along longitude 0°, airflow near the surface over West Africa is characterized by the simultaneous occurrence of the northeastern trade wind "Harmattan" and the monsoon flow from the southwest (Figures 1 of *Lacaux et al.* [1992] and *Fontan et al.* [1992]). The ITCZ associated with those two flow regimes gives rise to a strong gradient of moisture between the dry Saharan air advected by the Harmattan and the oceanic air of the monsoon flow. This front is located near latitude 8°N in January and close to 20°N in July [*Lacaux et al.*, 1992; *Fontan et al.*, 1992], as shown in Walker's diagram (Figure 1) (reproduced from *Cautenet and Rosset* [1989]).

In view of the intense seasonal variability of the West African circulations, we have chosen to study the transport of trace gases by means of two meteorological scenarios with initial fields corresponding to the January and July climatological averages, respectively.

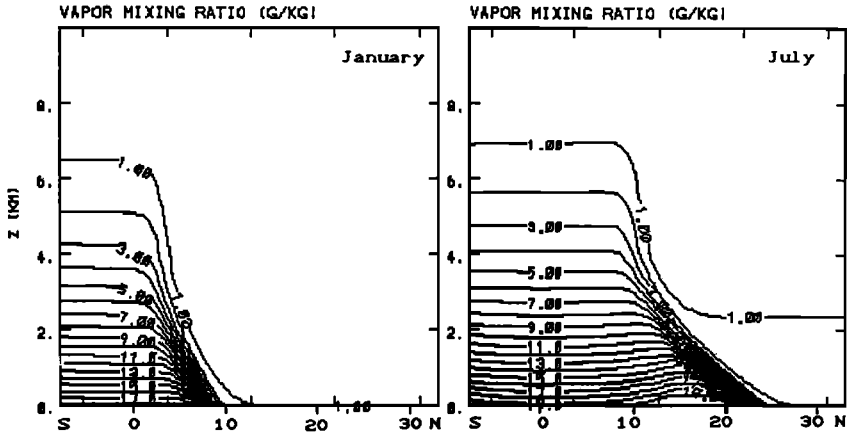

Figure 2. Vertical cross sections of the initial vapor mixing ratio in January and July.

3.1. Initial Fields

The initial distribution of the vapor mixing ratio deduced from *Reed et al.* [1977] and *Cadet and Nnoli* [1987] is shown in Figure 2. The initial upper limit of the saturated monsoon layer is marked by the strong horizontal gradient of moisture. As the front shifts southward with altitude, the monsoon layer is thicker in the south of West Africa [*Reed et al.*, 1977; *Dettwiller*, 1965]. We have also reproduced the seasonal variation of the ground location of the ITCZ by analytical variations of the initial vapor mixing ratio with latitude (Figure 2).

The initial meridional and zonal winds derived from *Burpee* [1972], *Reed et al.* [1977], *Newell and Kidson* [1984], and *Dettwiller* [1965] are presented in Figures 3 and 4, respectively. Thus we have modeled the monsoon flow (MF), characterized by western winds near the surface in Figure 4 and southern winds in Figure 3, with a maximum western wind speed at 3°N in July and at 0°N in January. The Harmattan (H) is represented by the northeasterly winds in the low levels of the northern part of the domain. The low-level convergence zone of the meridional wind (Figure 3) coincides with the ITCZ (Figure 2) and with the limit between the monsoon flow and the Harmattan in Figure 4.

The divergence at an altitude of 15 km and the convergence of the meridional wind at low levels in Figure 3 (the ITCZ) represent the northern and southern branches of the Hadley circulation. The northerly winds at upper levels of the right-hand part of Figure 3 represent the initial entrance zone of the subtropical jet in January.

In addition to the seasonal shift of the Hadley cells and the ITCZ we have also incorporated the seasonal variations of the West African low- and high-level jets. Figure 4 shows the initial representations in July of the African easterly jet (AEJ) (with maximum wind speeds of 8 m s^{-1} at 15°N and an altitude of 4 km), the tropical easterly jet (TEJ) (24 m s^{-1}, 8°N, 15 km altitude), and a low-level easterly jet in the south (5 m s^{-1}, 5°S, 4 km altitude). In January the TEJ is suppressed owing to the reversal of the temperature gradient between the Indian Ocean and the Tibetan plateau, and the intensity of the AEJ is reduced and shifted southward (3 m s^{-1}, maximum wind speed located at 5°N and 4 km in altitude). Also in January, the westerly subtropical jet (STJ) makes its appearance over West Africa (40 m s^{-1}, 21°N, 13 km in altitude).

3.2. The Meteorological Situation

The simulation starts at midnight and lasts 24 hours. Following *Fontan et al.* [1992], we have distinguished among five surface zones: ocean, forest, savanna, steppe, and desert. The associated latitudinal variations for latent and sensible heat fluxes have been represented by analytical functions of the horizontal position. Time variations of those

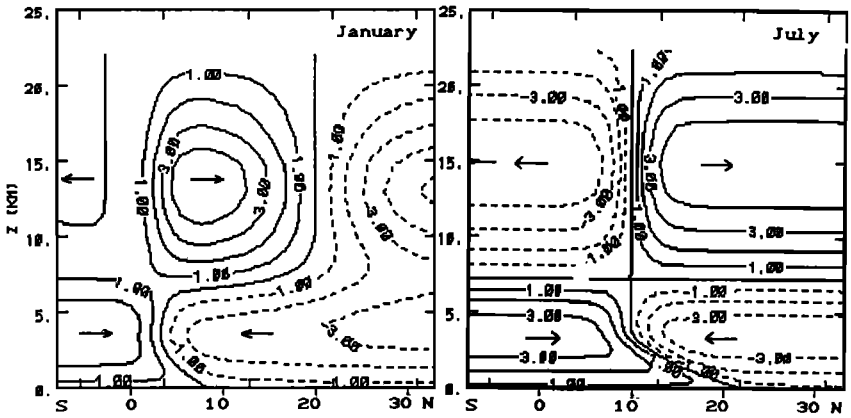

Figure 3. Vertical cross sections of the initial meridional wind in January and July.

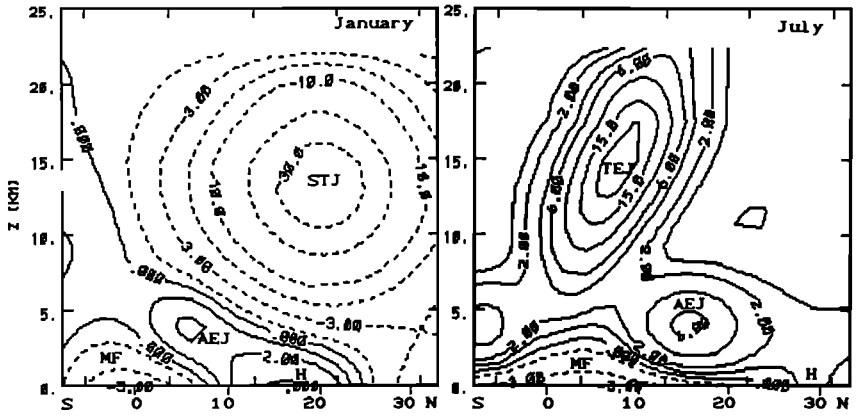

Figure 4. Vertical cross sections of the initial zonal wind showing the location of the main African jets (African easterly jet, south tropical jet, and tropical easterly jet) and the monsoon flux, the Harmattan flux in the low levels. January and July are represented.

surface fluxes reproduce the diurnal cycle: slightly negative values of sensible heat fluxes and vanishing latent heat fluxes are assumed during the night. A sinusoidal variation during the day leads to maximum heat fluxes at noon time. These maxima are deduced from *Da Fonseca Lyra* [1990] and *Cautenet et al.* [1992] and are indicated in Table 2.

The diurnal evolution of the meridional wind and the zonal wind after 9 hours is presented in Figures 5 and 6. A comparison of Figures 4 and 6 shows that the essential features of the zonal wind change little during the course of the simulation. Only some details evolve from the initial state: the low-level easterly jet is accelerated, the high-level jets are slowed down, and in July, high-level weak westerlies appear in the northern part of the domain.

The northern and the southern Hadley cells, represented by the meridional wind, change very little over that time period (Figures 3 and 5), and the position of the ITCZ remains stationary.

The stationarity of this meridional circulation has been obtained using the forcing term F_f in (7) in the inner parts of the domain. This forcing term also regulates the intensity of the meridional wind in the Hadley cells.

Updrafts occur near the equator in January and near 8°N in July in association with the ITCZ (Figure 7). In those regions, cloud masses of great vertical extent begin to form by 9 hours (Figure 8) and reach a state of maximum development at 15 hours. The cloudy region extends latitudinally from 2°S to 17°N in July and from 5°S to 5°N in January, in good agreement with the location of cloud tops over West Africa, as determined by IR satellite imagery [*Lacaux et al.*, 1992]. The seasonal differences in cloud water mixing ratios obtained at 15 hours indicate a greater cloud production mechanism in July and are consistent with enhanced convective activity observed during the rainy season.

In July we also notice the formation of stratified clouds at 15 hours from 5°N to 17°N at 2-km height associated with weak vertical ascents within the ITCZ at low levels (Figure 7). Moreover, the convective activity in July is not restricted to 8°N but extends from 2°N to 8°N, as can be seen from the cloudy masses at 15 hours in Figure 8 and on vertical velocities fields in Figure 7 at 9 hours. In fact, updrafts develop in the 2°N–5°N zone in July during the afternoon in response to the PBL convergence in the low levels near the limit between the ocean and the forest. These features are in agreement with the location of cloud tops, as determined by *Lacaux et al.* [1992]: convective activity extends farther in latitude in July than in January. This convective diurnal evolution highlights the fact that we really attempt in this paper to reproduce the transport of an inert tracer during a typical day of January or July with an initial state deduced from climatological averages.

Apart from a region of small upward vertical motion at 27°N in January due to friction effects and convergence of the meridional wind (Figure 6) the northern part of the domain is dominated by subsidence within the northern branch of the Hadley cell both in July and in January (Figure 7).

In concluding our discussion of this section, we note that the computed fields are mean values over the horizontal grid space and do not represent the actual highly variable fields associated with the real and individual convective clouds.

Table 2. Surface Maximum Latent and Sensible Heat Fluxes at 12 hours and Friction Velocity for the Different Surface Zones With Indication of Their Latitudinal Locations

Zone Definition	Ocean	Forest	Savanna	Steppe	Desert
Maximum sensible heat flux, W m^{-2}	5	300	400	300	400
Maximum latent heat flux, W m^{-2}	50	300	200	100	5
Friction velocity, m s^{-1}	0.02	0.6	0.4	0.4	0.2
Frontier location	5°N	8°N	11°N	20°N	

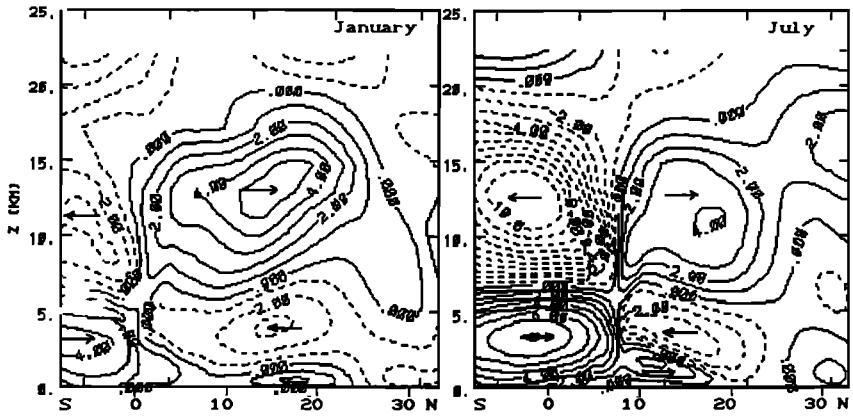

Figure 5. Vertical cross sections of the meridional wind after 9 hours of model time in January and July.

For example, the mean vertical velocity in the convective zone in July during the afternoon reaches 0.5 m s^{-1}. This value is lower than the 10 m s^{-1} of each individual cumulonimbus cloud but represents the mean vertical transport due to the actual clouds and is sufficient to form the cloudy masses we obtained. Despite this fact, the computed fields (in particular the vertical velocity and the cloud fields) appear to be in agreement with the observed mean ones [*Burpee*, 1972; *Reed et al.*, 1977; *Dettwiller*, 1965; *Newell and Kidson*, 1984]. This comparison with observations suggests that our model provides a reasonable depiction of the mean transport of trace gases in the convective zones of West African circulations.

4. The Inert Tracer Experiment

4.1. Results

We now show how the West African circulations described above affect the transport of a passive tracer such as carbon monoxide which has a very long residence time in the atmosphere. The initial vertical profile of the tracer is uniform over the entire domain and decreases exponentially with altitude, z (in meters), with an initial ground concentration of 400 ppb:

$$C(z) = C(0) \exp\left(-\frac{z}{2000}\right) \tag{17}$$

This ground concentration has been chosen to simulate the occurrence of savanna bush fires described by *Delmas et al.* [1991].

The temporal evolution of the tracer concentration $C(y, \nu, t)$ follows the equation

$$\frac{\partial \pi C}{\partial t} = -\frac{\partial UC}{\partial x} - \frac{\partial VC}{\partial y} - \frac{1}{\sigma'}\frac{\partial(\pi C \sigma' \nu)}{\partial \nu} + \pi F_{H,C} + \pi F_{V,C} \tag{18}$$

where $F_{H,C}$ represents the horizontal diffusion term and $F_{V,C}$ the vertical turbulent mixing effects of the planetary boundary layer. Hence no chemical source or sink terms appear with the tracer. The five terms from left to right on the right-hand side in (18) will be denoted $C1$, $C2$, $C3$, $C4$, $C5$ in the following to make a term analysis of the different contributions of the tracer redistribution. Equation (18) is solved at each time step (40 s) using the instantaneous wind fields.

Figure 9 shows a two-dimensional cross section of the

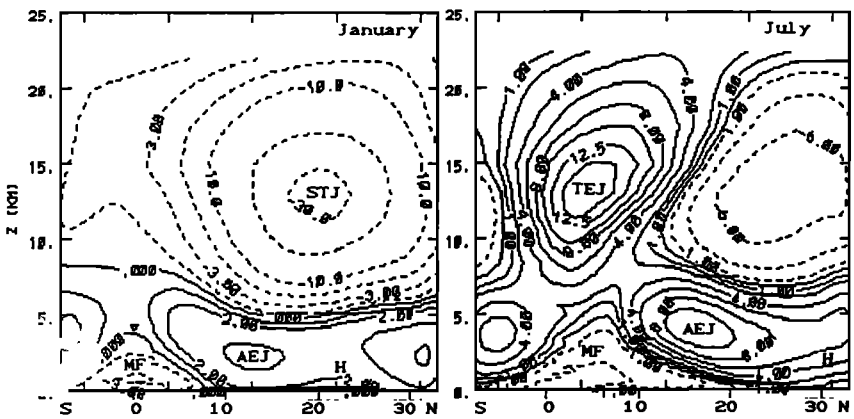

Figure 6. Vertical cross sections of the zonal wind after 9 hours of model time in January and July.

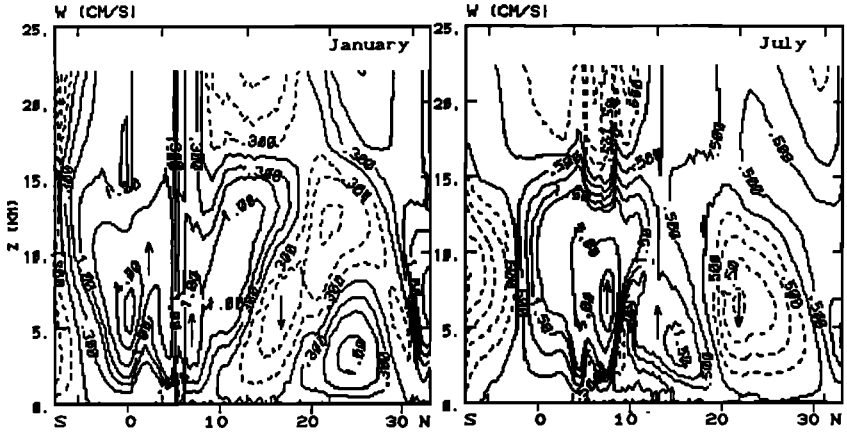

Figure 7. Vertical cross sections of the vertical velocity after 9 hours of model time. The vertical updrafts have a maximum of 7 cm s^{-1} in January and 13 cm s^{-1} in July, respectively.

inert tracer concentration after 24 hours of simulation in January and in July. We have indicated with dashed vertical lines two particular latitudes (2°N and 10°N) that have been selected because of their relative location versus the ITCZ, different between the dry and the wet seasons.

In the low levels and independently of the season the tracer is mixed by the PBL effects (term *C5*). This mixing is more pronounced and more extended vertically over the continent (northward of 5°N) than over the ocean (southward of 5°N), as can be seen from Figure 9. This effect of mixing is maximum, in fact, over the warm and sunny regions of the desert: in Figure 9 the concentration isocontour 100 ppb reaches 4 km in altitude and isocontours become more closely packed upward.

But the most important feature of the tracer transport in the low levels is its horizontal advection toward the ITCZ (term *C2*). This advection is due to the low-level parts of the Hadley cells: the meridional wind (Figure 5) converges toward the ITCZ region, advecting the tracer from the north, southward and the tracer from the south, northward. In Figure 9 we see that the convergence zone is characterized by an enhancement in the tracer concentration at a constant altitude (around 1 km) at 0°N in January and 3°N–5°N in July. This advection toward the ITCZ is also responsible for the reduction of the tracer concentration from the initial 400 ppb value during the 24-hour simulation near the ground in the northern part of the domain (Figure 9). In the southern regions this surface decrease even dominates the depletion due to the vertical mixing in the PBL.

The tracer that has been horizontally advected in the ITCZ is then transported upward by the updrafts in the boundary layer convergence zone and by the clouds. As already mentioned, the mean vertical velocity may reach up to 0.5 m s^{-1} in the afternoon in July in the cloudy masses. If we had considered only the boundary layer effects (term *C5*), the tracer would have remained below 3 or 4 km height, as previously described by *Chaumerliac et al.* [1992] and as can be deduced from the contrasting vertical evolution of the tracer between the cloudy and the noncloudy regions. The vertical transport by clouds (term *C3*), related to latent heat release effects, is the most efficient process and is shifted northward from January to July. The term *C3* in (18) is strengthened too by the forcing convergence of the Hadley cells (v in (10) is also due to $(\partial V_{div}/\partial y)$). The mean vertical transport of the tracer is clearly indicated in Figure 9 by enhanced values between 4 km and 8 km in altitude near the equator in January and 2°N–5°N in July. These regions of high concentration are related to the presence of cloudy masses (Figure 8) and are associated with the ITCZ.

For further insights of this vertical transport, we now present in Figure 10 the associated temporal evolution of the vertical profile of the tracer for two different latitudes (2°N and 10°N) already indicated in Figure 9.

At 2°N latitude in July the vertical profile is for the most part within the ITCZ cloudy regions where strong mean vertical velocities during the day (up to 0.5 m s^{-1}) lead to an increase in the tracer concentration in the middle and upper levels. Concentration amounts at 7–8 km in altitude are nearly half of the initial ground concentration. Within the ITCZ there is a strong convergence of the meridional wind which causes horizontal advection of the tracer at lower levels, as already observed in Figure 9, thereby resulting in no net depletion of tracer concentration in the planetary boundary layer.

In January the computed profiles at 2°N are located close to the edge of the cloudy zone. Therefore the maximum at 8 km and the minimum at 5 km are the results of a kind of cloud detrainment. It is inappropriate here to talk about cloud detrainment since we represent only one single cloudy mass, but this effect is a result of the vertical shear of the meridional wind in the cloudy regions of the ITCZ (Figure 5) and thereby has the appearance of a detrainment effect. At 5 km the meridional wind converges toward the ITCZ, carrying the tracer from low-concentration regions to the cloudy region and the updraft region of the ITCZ. However, at 7 km the meridional wind diverges and just the opposite effect occurs.

This vertical shear in the meridional wind leads in January to a larger area of high concentration at 7 km than at 5 km compared to July, as seen in Figure 9, and to an unusual vertical profile of the tracer close to the edge of the cloudy masses of the ITCZ at 2°N (Figure 10). This profile is unusual since a maximum of concentration appears at 7–8 km just above a minimum at 5 km, indicating that the tracer is not

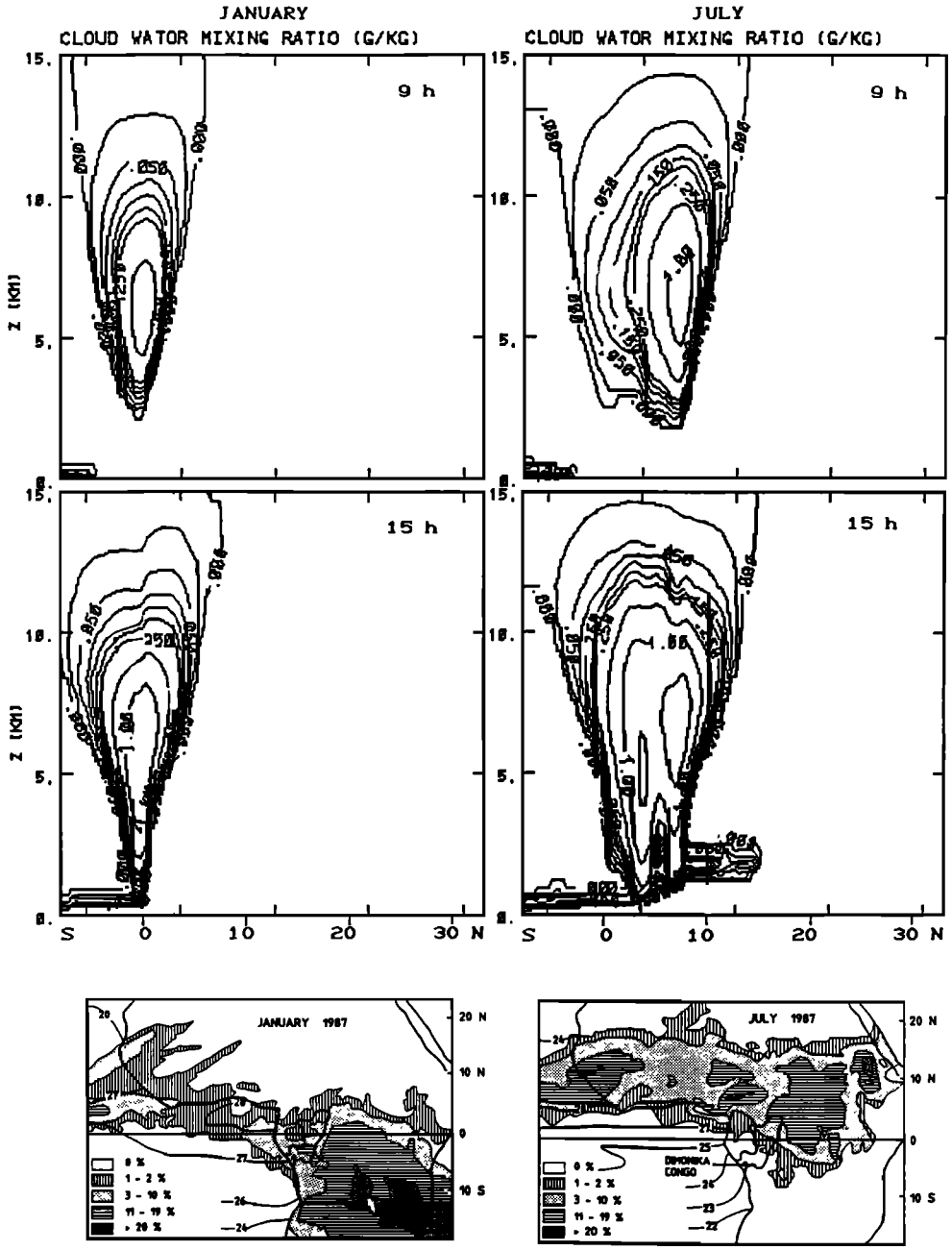

Figure 8. Vertical cross sections of the bulk cloud water mixing ratios after 9 and 15 hours of model time in January and July. The latitudinal extensions of cloudy regions are compared with satellite data (bottom part of the figure) presented by *Lacaux et al.* [1992].

directly transported from the ground to 7–8 km at a constant latitude. In fact, the tracer is first advected horizontally near the ground in the ITCZ, then it is lifted upward within the ITCZ at 0°N, and finally released from the ITCZ at 7–8 km near 2°N by the northward meridional wind. The efficiency of this mechanism depends upon the distance from the core of the ITCZ. The meridional wind needs more than 24 hours to advect the tracer at 10°N from the ITCZ at 7–8 km in January, thus no maximum appears in Figure 10 at 10°N in January. In July the northward shift of the ITCZ reduces the distance from the 10°N latitude and the core of the ITCZ, hence a maximum in the upper part of the profile forms at 10°N but with a smaller contrast in comparison with the situation at 2°N in January. Hence the seasonal variations of the tracer transport are primarily due to the northward shift of the ITCZ and to the increase of convective activity in July.

4.2. Discussion

The inert tracer experiment developed in the present paper highlights the specific role of dynamics on trace gases emitted by bush fires over West African savannas. Referring to our results, these trace gases may be first advected southward into the ITCZ, then vertically transported by

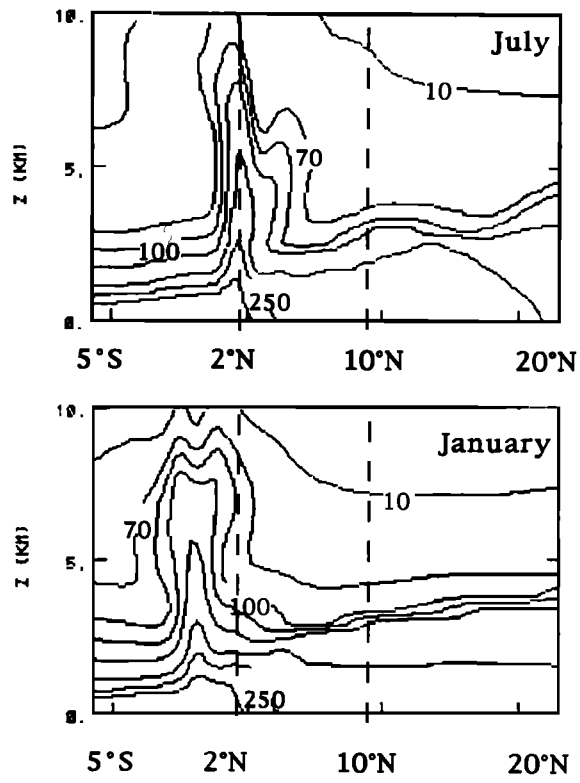

Figure 9. Vertical cross sections of the tracer concentration after 24 hours of model time in January and July.

convective activity within the ITCZ clouds, and finally, ejected at the high levels of the Hadley cells in a concentrated layer at 7–8 km in height at the edges of the ITCZ cloudy regions.

In our simulation of January at 2°N the tracer attains high concentrations in the first two kilometers, a local minimum near 5 km, and a local maximum between 6 km and 8 km. Such a vertical distribution has been reported by *Marenco et al.* [1990] during the TROPOZ I experiment in December 1987, with vertical cross sections of CO and O_3 between 6°S and 45°N. Our results give a simple and possible explanation for the maximum at 6–8 km in Abidjan (5°15N–3°54W) observed by Marenco: this vertical profile may be due to a purely dynamical effect of the global "detrainment" of the cloudy region of the ITCZ by the vertical shear of the meridional wind after the efficient upward transport of the biomass burning emissions by convective clouds of the ITCZ. The fact that O_3, which is not a passive tracer, exhibits the same behavior as CO [*Marenco et al.*, 1990] implies that the dynamical effects of clouds and the boundary layer convergence of the meridional wind may be the dominant mechanisms affecting the vertical redistribution of chemical species in that region.

However, a feature often observed during DECAFE (especially for ozone at low levels over the forest) is a maximum at 2–3 km and a depletion of concentrations near the surface [*Marenco et al.*, 1990; *Cros et al.*, 1991; *Andreae et al.*, 1992]. Such profiles have also been noticed over Amazonia (ABLE 2A, *Garstang et al.* [1988]). In that case, *Pickering et al.* [1991] have suggested that the existence of storm clouds "may temporarily prevent the daytime increase of ozone concentrations in the mixed layer, because deposition to the surface may exceed the net photochemical production rate under the cloud." In the African case, *Cros et al.* [1991] and *Fontan et al.* [1992] have suggested that at the juncture of the northern trade winds and the monsoon flow, the dry and polluted air advected by the northern trade winds surmounts the clean air of the monsoon flow [*Cros et al.*, 1991]. Hence the surface depletion may also follow the sloping frontal surface of the ITCZ.

Our numerical simulations do not reproduce such depletion near the ground in the first two kilometers of the polluted layer. If deposition effects and photochemical effects are responsible for this depletion, they cannot be accounted for since we consider only an inert tracer. For the depletion by the sloping frontal surface of the ITCZ this effect is inhibited by the initial uniform horizontal concentrations of the tracer used in this paper.

5. Conclusion

In this paper our aim was to study the influence of West African circulations at 0° longitude on the redistribution of atmospheric chemical compounds. We used a two-dimensional primitive equation model to simulate the primary features of observed meteorological fields. The location and spatial extent of cloud systems associated with the ITCZ were well represented by the model simulations, thereby providing a proper framework for the realistic transport of chemical species.

We focused on the vertical and horizontal transport of an inert tracer to highlight the specific role of dynamics, especially mean cloud dynamics on the distribution of chemical species in the tropical troposphere.

We have shown that an inert tracer is transported efficiently from the surface to the middle and upper troposphere by the mean vertical velocity within the cloudy masses of the ITCZ. Furthermore, we found that the vertical shear of the meridional wind nominally associated with the presence of the Hadley cell within the cloudy regions of the ITCZ lead to a maximum in the chemical tracer concentration at an elevation of 6 to 8 km at the edges of the ITCZ. This layer is clearly separated from the lower maxima near the ground by a layer of minimum tracer concentration at an elevation of 5 km. These results are in good agreement with other references in the literature and suggest that the lower branch of the northern Hadley cell advects the chemical species emitted by bush fires during the dry season of the northern hemisphere toward the ITCZ. Later, the vertical motions and the meridional wind associated with the ITCZ act to increase the concentrations at higher levels in the atmosphere.

By comparing results obtained in January and July, we have also shown that the redistribution of the inert tracer is closely related to the seasonal migration of the ITCZ. This work represents merely a preliminary step in the study of the redistribution of chemical species by West African circulations and ITCZ clouds. Further developments should include chemical and depositional processes in order to obtain more realistic and quantitative comparisons with experimental data.

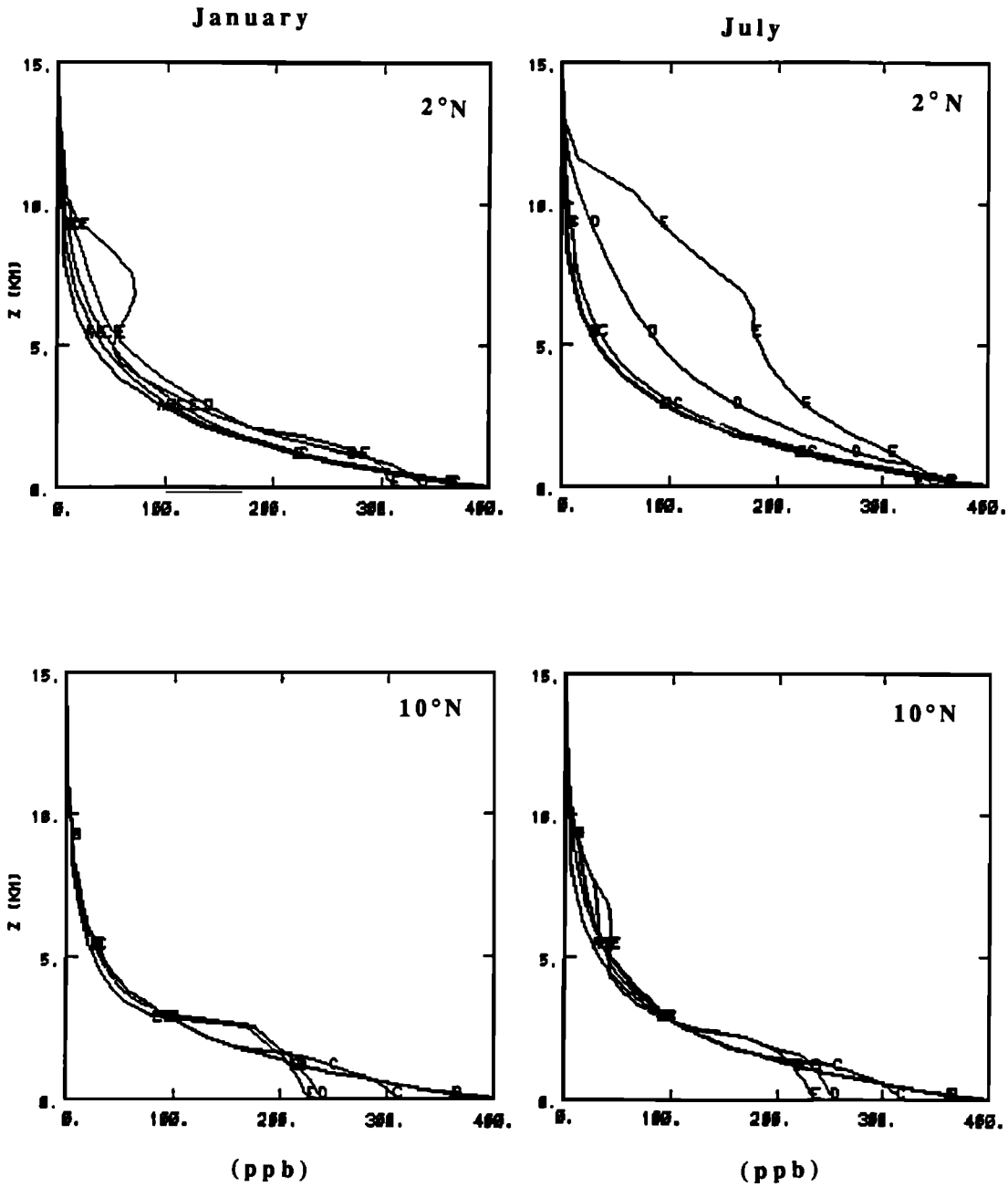

Figure 10. Vertical profiles for an inert tracer with a homogeneous initial ground concentration of 400 ppb all over the model domain. These profiles are drawn for 2°N and 10°N in latitudes, in January and July. Curve A is the initial profile and curves B, C, D, and E are the profiles at 6, 12, 18, and 24 hours of model time, respectively.

Appendix

The forcing meridional wind $V_{def} + V_{div}$ has been selected to model two main features of the West African circulations: the convergent and divergent zones of the Hadley cells and the entrance or exit zones of the zonal jets.

In section 3.1 and in Figure 3 the resulting meridional wind has been already presented. Its divergent part, V_{div}, is, in fact, the superposition of two different divergent fields associated with the low-level convergence and the high-level divergence, respectively, of the ITCZ. Each of those fields has the same following form:

$$V_{div} = V_c(\nu) th\left(\frac{y - y_c(\nu)}{\delta y_c}\right) \tag{A1}$$

where $th(x)$ is the hyperbolic tangent of the variable x. $V_c(\nu)$ is the vertical profile of the wind intensity. $V_c(\nu)$ is negative everywhere and vanishes above 7 km in altitude for the low-level convergence field: $y_c(\nu)$ is the center of convergence or divergence at level ν and follows the vertical slope of the ITCZ under 3.5 km (Figure 3); and δy_c is the length of the divergent zone.

In the same manner, the nondivergent part of the meridi-

onal wind V_{def} is the superposition of two different deformation fields associated with the entrance or exit zones of the low-level jet AEJ or of the high-level jet (TEJ or STJ, depending on the season which is considered). To make each of these meridional winds V_{def} nondivergent, we have associated a zonal wind U_{def} satisfying (5). Generally, the deformation field of Bergeron is chosen as $U_{def} = -\alpha x$, $V_{def} = \alpha(y - y_d)$, where y_d is the center of deformation and α the deformation parameter. Unfortunately, this formulation leads to nonrealistic high values of V_{def} far from the center of deformation and prevents from variations of the intensity of the deformation with height.

To reproduce more precisely the horizontal and vertical location of the entrance or exit zones of the jets, we have chosen the following form for each deformation field:

$$U_{def} = -V_d(\nu)\frac{\delta x_d}{\delta y_d} th\left(\frac{x}{\delta x_d}\right)\left(1 - th^2\left(\frac{y - y_d(\nu)}{\delta y_d}\right)\right) \quad \text{(A2)}$$

$$V_{def} = V_d(\nu)\left(1 - th^2\left(\frac{x}{\delta x_d}\right)\right)th\left(\frac{y - y_d(\nu)}{\delta y_d}\right) \quad \text{(A3)}$$

where $V_d(\nu)$ represents the vertical profile of the wind intensity, hence the deformation intensity, $y_d(\nu)$ the center of deformation at level ν, δx_d and δy_d the longitudinal (zonal) and the transverse (meridional) lengths of the deformation zone, respectively. U_{def}, V_{def} are solution of (5) in the ν vertical coordinate system for the variables $U = \pi u$ and $V = \pi v$.

Following the classical formulation of Bergeron and its use in the semigeostrophical approximation [*Hoskins and Bretherton*, 1972], we have assumed that U_{def} vanishes in the cross-section plane of the model ($x = 0$ in (A3)). This assumption ensures simplifications in the calculation of the initial zonal wind.

Acknowledgment. The authors would like to thank R. Rosset for many informative discussions we had concerning this work.

References

Andreae, M. O., A. Chapuis, B. Cros, J. Fontan, G. Helas, C. Justice, Y. K. Kaufman, A. Minga, and D. Nganga, Ozone and Aitken nuclei over equatorial Africa: Airborne observations during DECAFE 88, *J. Geophys. Res.*, *97*, 6137–6178, 1992.

Burpee, R. W., The origin and the structure of easterly waves in the lower troposphere of North Africa, *J. Atmos. Sci.*, *29*, 37–50, 1972.

Cadet, D., and N. O. Nnoli, Water vapour transport over West Africa and the Atlantic Ocean during summer 1979, *Q. J. R. Meteorol. Soc.*, *113*, 581–602, 1987.

Cautenet, S., and R. Rosset, Numerical simulation of sea breezes with vertical wind shear during dry season at Cape of Three Points, West Africa, *Mon. Weather Rev.*, *117*, 329–339, 1989.

Cautenet, G., M. Legrand, and S. Cautenet, Thermal impact of Saharan dust over land, I, Simulation, *J. Appl. Meteorol.*, *31*, 166–179, 1992.

Chatfield, R. D., and P. J. Crutzen, Sulfur dioxide in remote oceanic air: Cloud transport of reactive precursors, *J. Geophys. Res.*, *89*, 7111–7132, 1984.

Chatfield, R. D., and A. C. Delany, Convective links biomass burning to increased tropical zone: However, models will tend to overpredict O_3, *J. Geophys. Res.*, *95*, 18,473–18,468, 1990.

Chaumerliac, N., R. Rosset, M. Renard, and E. C. Nickerson, The transport and redistribution of atmospheric gases in regions of frontal rain, *J. Atmos. Chem.*, *14*, 43–51, 1992.

Cros, B., D. Nganga, R. Delmas, and J. Fontan, Tropospheric ozone and biomass burning in intertropical Africa, in *Global Biomass Burning*, edited by J. Levine, pp. 42–45, MIT Press, Cambridge, Mass., 1991.

Crutzen, P. J., A. C. Delany, J. Greenberg, P. P. Haagenson, L. Heidt, R. Lueb, W. Pollock, W. Seiler, A. Wartburg, and P. Zimmerman, Photochemically produced ozone in the emission from large-scale tropical vegetation fires, *J. Geophys. Res.*, *90*, 2425–2429, 1985.

Da Fonseca Lyra, R., Dynamique et transferts dans et au-dessus des couverts forestiers, thèse d'université, Toulouse, France, 1990.

Davies, H. C., Limitations of some common lateral boundary schemes used in regional NWP models, *Mon. Weather Rev.*, *111*, 1002–1012, 1983.

Delmas, R., On the emission of carbon, nitrogen and sulfur in the atmosphere during bushfires in intertropical savannah zones, *Geophys. Res. Lett.*, *9*, 761–764, 1982.

Delmas, R., P. Lodjani, A. Podaire, and J. C. Menaut, Biomass burning in Africa: An assessment of the annually burned biomass, in *Global Biomass Burning*, edited by J. Levine, pp. 60–67, MIT Press, Cambridge, Mass., 1991.

Dettwiller, I., Note sur la structure du FIT boréal sur le Nord-Ouest de l'Afrique, *La Météorologie*, *VI*, *80*, 337–347, 1965.

Fontan, J., A. Druilhet, B. Benech, Lyra, R., and B. Cros, The DECAFE experiments: Overview and meteorology, *J. Geophys. Res.*, *97*, 6123–6136, 1992.

Garstang, M., et al., Trace gas exchanges and convective transports over the Amazonian rain forest, *J. Geophys. Res.*, *93*, 1528–1550, 1988.

Harris, R. C., et al., The Amazon Boundary Layer Experiment (ABLE 2A), Dry season 1985, *J. Geophys. Res.*, *93*, 1351–1360, 1988.

Hoskins, B. J., and F. P. Bretherton, Atmospheric frontogenesis models: Mathematical formulation and solution, *J. Atmos. Sci.*, *29*, 11–37, 1972.

Hsie, E. Y., R. A. Anthes, and D. Keyser, Numerical simulation of frontogenesis in a moist atmosphere, *J. Atmos. Sci.*, *41*, 2581–2594, 1984.

Kessler, E., On the redistribution and continuity of water substance in atmospheric circulations, *Meteorol. Monogr.*, *10*(32), 84, 1969.

Lacaux, J. P., R. Delmas, G. Kouadio, B. Cros, and M. O. Andreae, Precipitation chemistry in the Mayombe forest of equatorial Africa, *J. Geophys. Res.*, *97*, 6195–6206, 1992.

Mahfouf, J. F., E. Richard, P. Mascart, and E. C. Nickerson, A comparative study of various parameterizations of the planetary boundary layer in a numerical mesoscale model, *J. Clim. Appl. Meteorol.*, *26*, 1671–1695, 1987.

Marenco, A., J. C. Medale, and S. Prieur, Study of tropospheric ozone in the tropical belt (Africa, America) from STRATOZ and TROPOZ campaigns, *Atmos. Environ.*, *24*(A), 2823–2834, 1990.

Newell, R. E., and J. E. Kidson, African mean wind changes between Sahelian wet and dry periods, *J. Climatol.*, *4*, 27–33, 1984.

Nickerson, E. C., E. Richard, R. Rosset, and D. R. Smith, The numerical simulation of clouds, rain and airflow over the Vosges and Black Forest Mountains: A meso-β model with parameterized microphysics, *Mon. Weather Rev.*, *114*, 398–414, 1986.

Pickering, K. E., Thompson, A. M., J. Scala, W. K. Tao, J. Simpson, and M. Garstang, Photochemical ozone production in tropical squall lines convection during NASA Global Tropospheric Experiment/ABLE 2A, *J. Geophys. Res.*, *96*, 3099–3114, 1991.

Reed, R. J., D. C. Norquist, and E. E. Recker, The structure and properties of African waves disturbances as observed during phase III of GATE, *Mon. Weather Rev.*, *105*, 317–333, 1977.

Richard, E., and N. Chaumerliac, Effects of different rain parameterizations on the simulation of mesoscale orographic precipitation, *J. Appl. Meteorol.*, *28*, 1197–1212, 1989.

Therry, G., and P. Lacarrère, Improving the eddy kinetic energy model for planetary boundary layer description, *Boundary Layer Meteorol.*, *25*, 63–88, 1983.

S. Cautenet, N. Chaumerliac, and M. Renard, LAMP/OPGC, Université Blaise Pascal, 24, Avenue des Landais, 63177 Aubiere Cedex, France.

E. C. Nickerson, National Oceanic and Atmospheric Administration/FSL, Boulder, CO 80303.

(Received February 25, 1993; revised February 11, 1994; accepted February 11, 1994.)